

FURTHER DEVELOPMENTS IN STRESS INITIALIZATION IN GEOMECHANICS VIA FEM AND A TWO-STEP PROCEDURE INVOLVING AIRY FUNCTIONS

C.R. YBERN^{*}, I. JAQUÉS^{*}, I. ALIGUER^{*}, I. CAROL^{*}, P.C. PRAT^{*},
M.R. LAKSHMIKANTHA[†], J.M. SEGURA[†]

^{*} ETSECCPB (School of Civil Engineering)
Universitat Politècnica de Catalunya (UPC)
Campus Nord UPC, 08034 Barcelona, Spain
e-mail: ignacio.carol@upc.edu

[†] Repsol Technology Hub
The Woodlands, TX 77381, USA
e-mail: m.lakshmikantha@repsol.com

Key words: *In-situ* stress, initialization stress function, Finite Element Method (FEM), Oil & Gas.

Abstract.

The *in-situ* stress field in rock masses is a key aspect when a numerical analysis of a rock mass is carried out in any area of geo-engineering, such as civil, mining, or Oil & Gas. A method for the numerical generation of the *in-situ* stress state in the FE context, based on Airy stress functions was previously introduced. It involves two steps: 1) an estimate of the stress state at each Gauss point is generated, and 2) global equilibrium is verified and re-balancing nodal forces are applied as needed. In this paper, new developments towards improving the accuracy of the stress proposal are discussed. A real application example has been used to illustrate the results achieved with the new implementation.

1 INTRODUCTION

Geological materials are inevitably subject to an in situ stress field which is crucial for the evaluation of the geomechanical response of the rock mass in a variety of fields of Engineering [1,2]. However, in-situ measurement procedures are complex and expensive, and their accuracy strongly depends of every type of situation. Additionally, although in-situ measurements are certainly essential, stress fields are also subject to some constraints due to physical laws such as equilibrium and limit behaviour of material laws. For this reason, it is nowadays accepted that a sound procedure to reconstruct an accurate picture of the in-situ stress field requires the combination of measurements with numerical calculations [3].

Ideally, the in-situ stress state could be obtained by modelling the complete geological history of the rock mass. However, the realistic analysis of that history would be in general too complex, or the geological history may not be known exactly. This is why the strategy is changed to simply trying to obtain the “current picture” of the stress state in the rock mass, using simplified procedures.

In previous papers [4,5], the authors have discussed the equations to be satisfied by the initial stress field, and have proposed a two-step method to generate in-situ stress states which was based on Airy functions and the Finite Element method. In the first step, a first estimate of the stress state or “guess” at each Gauss point is proposed using vertical stresses due to gravity and horizontal due to the so-called horizontal to vertical stress ratio (K), and in a second step global equilibrium is verified and re-balancing nodal forces are applied as needed.

In this paper, further developments accomplished in this procedure are described, which include a non-linear based redistribution of unbalanced nodal forces and a parametric description of the geometry of the subdomains of interest. As the result of these new developments, the method is now more suitable for more complex geometries and situations, and also these changes are crucial for the extension of the method to 3D problems. The procedure described is illustrated with an example of application to a real reservoir field.

2 GENERATION OF THE INITIAL STRESS PROPOSAL σ^{prop} BASED ON STRESS FUNCTIONS

This method is based on the use of the so-called stress functions $\Phi(x, y, z)$, from which the components of the stress tensor are derived as follows:

$$\sigma_{ij} = F_{ij}\{\Phi\}, \quad (1)$$

where F_{ij} is a differential operator and Φ is a scalar function of x , y and z . In the particular case of two-dimensional analysis, the expression reduces to:

$$\sigma_{xx} = \frac{\partial^2 \Phi}{\partial z^2} + \sigma_{xx0} \quad (2)$$

$$\sigma_{zz} = \frac{\partial^2 \phi}{\partial x^2} - \gamma z + \sigma_{zz0}$$

$$\sigma_{xz} = \frac{\partial^2 \phi}{\partial x \partial z} + \sigma_{xz0}.$$

and $\Phi(x, z)$ is known as the Airy stress function [6-7]. In our particular case, a third degree polynomial expression with constant coefficients is used as stress function:

$$\Phi(x, z) = \frac{a_1}{6} x^3 + \frac{a_2}{2} x^2 z + \frac{a_3}{2} x z^2 + \frac{a_4}{6} z^3. \quad (3)$$

which leads to linear expressions of stress components in terms of the geometrical coordinates (x, z) and the coefficients a_i , which need to be determined via minimization procedure.

In order to determine the unknown coefficients, the entire domain is decomposed into vertical or sub-vertical strips, that are in turn subdivided into trapezoidal subdomains (Fig. 1-Left).

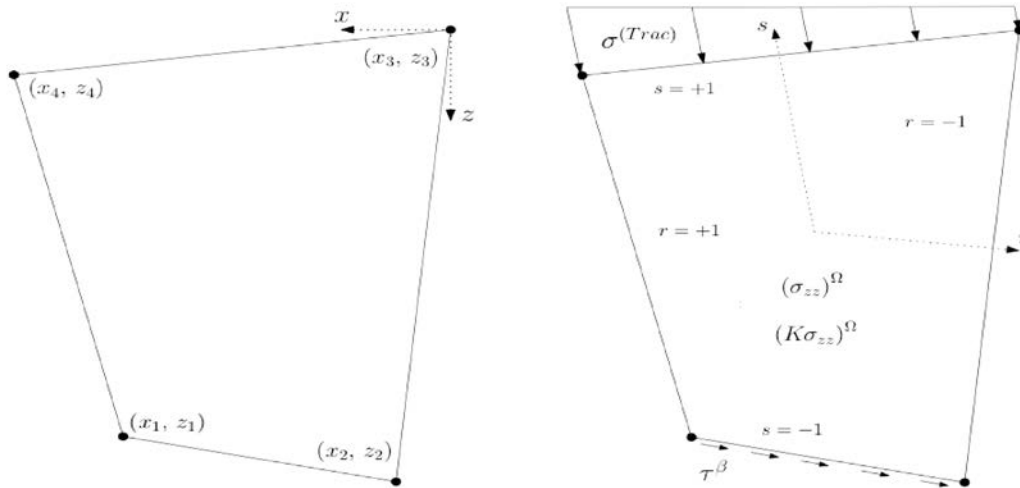


Figure 1 – (Left) Geometric definition of a linear prismatic subdomain and boundaries in the coordinates (x, z) . (Right) The boundary conditions: $\bar{\sigma}^{(Trac)}$ $\bar{\tau}^{(\beta)}$ and $\bar{\sigma}_{yy}$ in parametrized (r, s) subdomain.

The coordinates (x, z) of each subdomain may be expressed *via* interpolation of the nodal coordinates of the subdomain through linear interpolation functions N_i , i.e. $x = \sum_{i=1}^4 N_i(r, s) x_i$ and $z = \sum_{i=1}^4 N_i(r, s) z_i$. This leads to the stress components in the subdomain in terms of the natural coordinates of the subdomain (r, s) as follows:

$$\sigma_{xx} = a_3 \sum_{i=1}^4 N_i(r, s) x_i + a_4 \sum_{i=1}^4 N_i(r, s) z_i + \sigma_{xx0} \quad (4)$$

$$\sigma_{zz} = a_1 \sum_{i=1}^4 N_i(r, s) x_i + (a_2 - \gamma) \sum_{i=1}^4 N_i(r, s) z_i + \sigma_{zz0}$$

$$\sigma_{xz} = -a_2 \sum_{i=1}^4 N_i(r, s) x_i - a_3 \sum_{i=1}^4 N_i(r, s) z_i + \sigma_{xz0}.$$

where the initial stress values $\sigma_{xx0}, \sigma_{zz0}, \sigma_{xz0}$ can be considered as additional subdomain parameters (a_i , $i = 5, 6, 7$) to be included in the minimization procedure.

The subdomains on each vertical strip are considered sequentially from top to bottom. Each subdomain is limited on the top and bottom by edges corresponding to $s = +1$ and $s = -1$ respectively. Also, left and right edges are given by $r = -1$ and $r = +1$. These edges are plane but not necessarily horizontal, and are subject to the following boundary conditions: 1) The components of traction vector ($\bar{\sigma}^{(Trac)}$) on the top edge ($s = +1$) is prescribed as a linear function of x and z . 2) Vertical stress gradient ($\bar{\sigma}_{zz}$) on entire surface is also prescribed as a linear function of x and z . 3) The shear intensity ($\bar{\tau}^{(\beta)}$) on the bottom edge ($s = -1$) is linked to the amount of normal stress on the same edge. 4) Horizontal stress ($\bar{\sigma}_{xx}$) on entire domain and is related to vertical stress σ_{zz} via K .

According to the boundary conditions imposed on the top and bottom edges and the entire surface of the subdomain (Fig. 1-Right), an objective function $G(a_i)$ is considered for the subdomain that integrates the square difference between: 1) the traction vector components and its prescribed values, 2) the shear stresses and its prescribed values, 3) the horizontal stress component and K times the prescribed vertical stress values, and 4) the vertical stress components and its prescribed values. Considering the derivatives of the objective function with respect to the coefficients a_i , then the stress state that best fits the boundary conditions is defined by the parameters (a_i) that minimize the objective function:

$$\begin{aligned} \frac{\partial G}{\partial a_i}(a_i) = & \frac{\partial}{\partial a_i} \int_{-1}^{+1} \sum_{i=1}^n (\sigma^{(Trac)} - \bar{\sigma}^{(Trac)})^2 J^{(s=+1)} dr + \\ & + \frac{\partial}{\partial a_i} \int_{-1}^{+1} (\tau^{(\beta)} - \bar{\tau}^{(\beta)})^2 J^{(s=-1)} dr + \\ & + \frac{\partial}{\partial a_i} \iint_{-1}^{+1} (\sigma_{xx} - K \bar{\sigma}_{zz})^2 J^{(r,s)} dr ds + \\ & + \frac{\partial}{\partial a_i} \iint_{-1}^{+1} (\sigma_{zz} - \bar{\sigma}_{zz})^2 J^{(r,s)} dr ds, \end{aligned} \quad (5)$$

wherein $J^{(c)}$ is the determinant of the Jacobian of the coordinates transformation (global to natural) at the corresponding boundary and n is the number of components of traction vector.

$\sigma^{(Trac)}$, $\tau^{(\beta)}$ are the traction vector and shear stress of the proposed distribution on the top and bottom edges of the subdomain with the corresponding prescribed values $\bar{\sigma}^{(Trac)}$ and $\bar{\tau}^{(\beta)}$. σ_{zz} and σ_{xx} are the corresponding stress components evaluated on entire surface and $\bar{\sigma}_{zz}$ is the vertical stress prescribed nodal value.

3 APPLICATION TO A REAL RESERVOIR CROSS-SECTION

The example of application of the procedure described consists of the real geological 2D cross-section shown in Fig. 2-top.

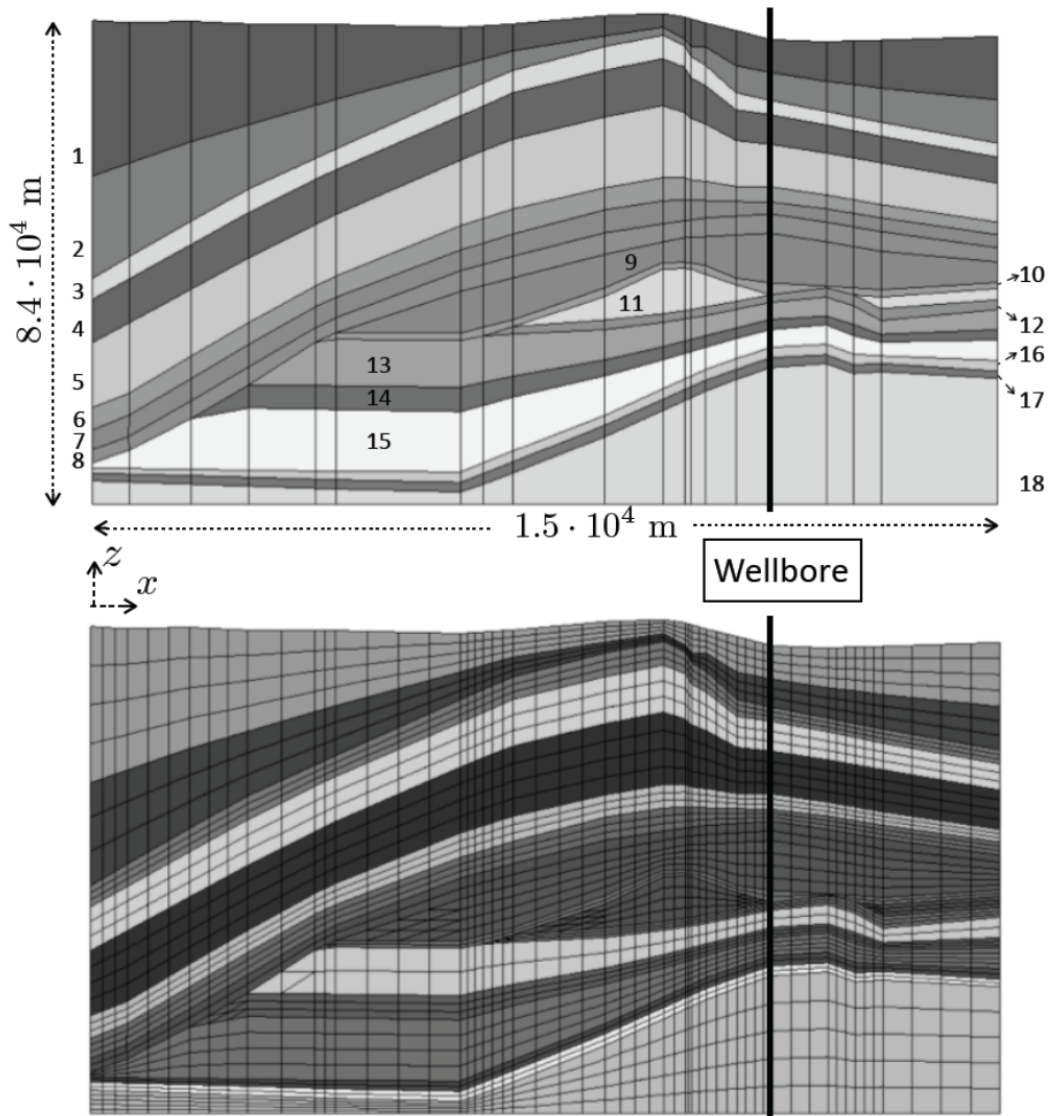


Figure 2 - (Top) Geomechanical model. (Bottom) Finite Element Mesh of the cross-section. The thick vertical line indicates location of a wellbore.

The geometry of the geological formation is very adequate for 2D analysis since all the cross-sections parallel to the one considered have a very similar geometry. Furthermore, the cross-section considered has the advantage of the availability of field measurements from a wellbore. The following data is available: Young's modulus (E), Poisson's ratio (ν), rock density (ρ), fluid pore pressure (P_f), and horizontal-to-vertical stress ratio (K). Table 1 shows these parameters for each layer of the domain (top to bottom).

In order to apply the procedure based on Airy stress functions, the domain is subdivided in a total of 22 vertical stripes, and each of these layers is in turn subdivided into a number of trapezoids by intersection with the 18 geological layers, as also shown in Fig.2-top. Once the geometrical model is established, a FE mesh is generated as depicted in Fig. 2-bottom, with a total of 2899 quadratic elements (2816 quadrangles and 83 triangles), and 8822 nodes.

As previously mentioned, a nonlinear behaviour has been assumed for the rock mass. The use of this type of constitutive behaviour allows the redistribution of excessive and usually unrealistic stress values that typically appear near surface in valleys or other geometries when a pure elastic analysis is carried out. In particular, a simplified elastic perfectly-plastic constitutive law with a hyperbolic Drucker-Prager [8] yield criterion is assumed as follows:

$$F = \sqrt{J_2} - \tan \varphi^f \sqrt{p^2 + \left(\frac{c^f}{\tan \varphi^f} - t_p^f \right)}, \quad (6)$$

where p is the first invariant of the stress tensor, $\sqrt{J_2}$ is the second invariant of the deviatoric tensor, φ^f is the friction angle, c^f is the cohesion and t_p^f is the tensile strength. Also associated plasticity ($F = Q$) has been considered in the present example, as shown in Fig. 3. Values of $c^f = 100\text{kPa}$, $\varphi^f = 30^\circ$ and $t_p^f = 50\text{kPa}$, which are standard in the literature of Rock Mechanics have been used to characterize the non-linear response of the rock mass.

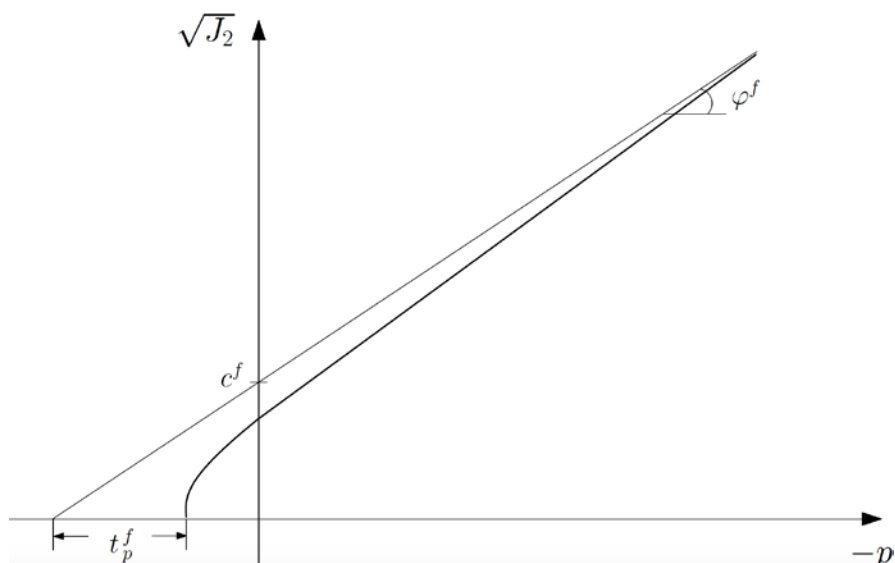


Figure 3 - A simplified elastic perfectly-plastic constitutive law with a hyperbolic Drucker-Prager [8].

Table 1: Values of different parameters used in each layer in the geometry model

Layer	Young (GPa)	Specific weight	Poisson	K
1	13.79	24.13	0.224	2.14
2	27.23	25.21	0.23	1.93
3	22.75	25.11	0.227	1.27
4	19.99	24.33	0.22	1.06
5	31.03	25.51	0.235	1.14
6	44.82	25.90	0.235	1.31
7	37.92	24.82	0.24	1.16
8	46.88	25.41	0.25	1.27
9	17.24	24.13	0.233	1.09
10	42.75	25.02	0.25	1.14
11	49.64	25.80	0.253	1.17
12	46.88	25.80	0.22	1.20
13	39.99	25.02	0.244	1.15
14	43.78	25.11	0.245	1.19
15	37.92	25.21	0.24	1.21
16	51.71	25.90	0.25	1.19
17	31.03	25.21	0.245	1.24
18	42.75	25.02	0.25	1.14

The elastic rock properties assigned to each geomechanical unit are listed in Table 1. The results obtained, are presented in Fig. 4 in terms of both total and effective vertical and horizontal stress profiles along the wellbore.

In Fig. 4, dotted-dashed lines represent the stress profiles resulting from the stress proposal based on the Airy functions (step 1 of the procedure). Solid lines represent the equilibrated stress profiles, obtained after the application of the unbalanced nodal forces (step 2). As it can be observed in the figure, the equilibrated stress states exhibit a better agreement with the previous available data along the well (dashed line). Overall, this agreement with available data is remarkable in both horizontal and vertical stress components and the general trend and also local effects are captured. However, vertical stress profile shows a better fit in the upper 3500 m, which is the main area of interest since it corresponds to the reservoir and the overburden.

Since all calculations have been carried out in terms of total stresses, the profiles in terms of effective stresses have been obtained via a post-processing using the available fluid pressure along the wellbore, as shown in Fig.4-bottom.

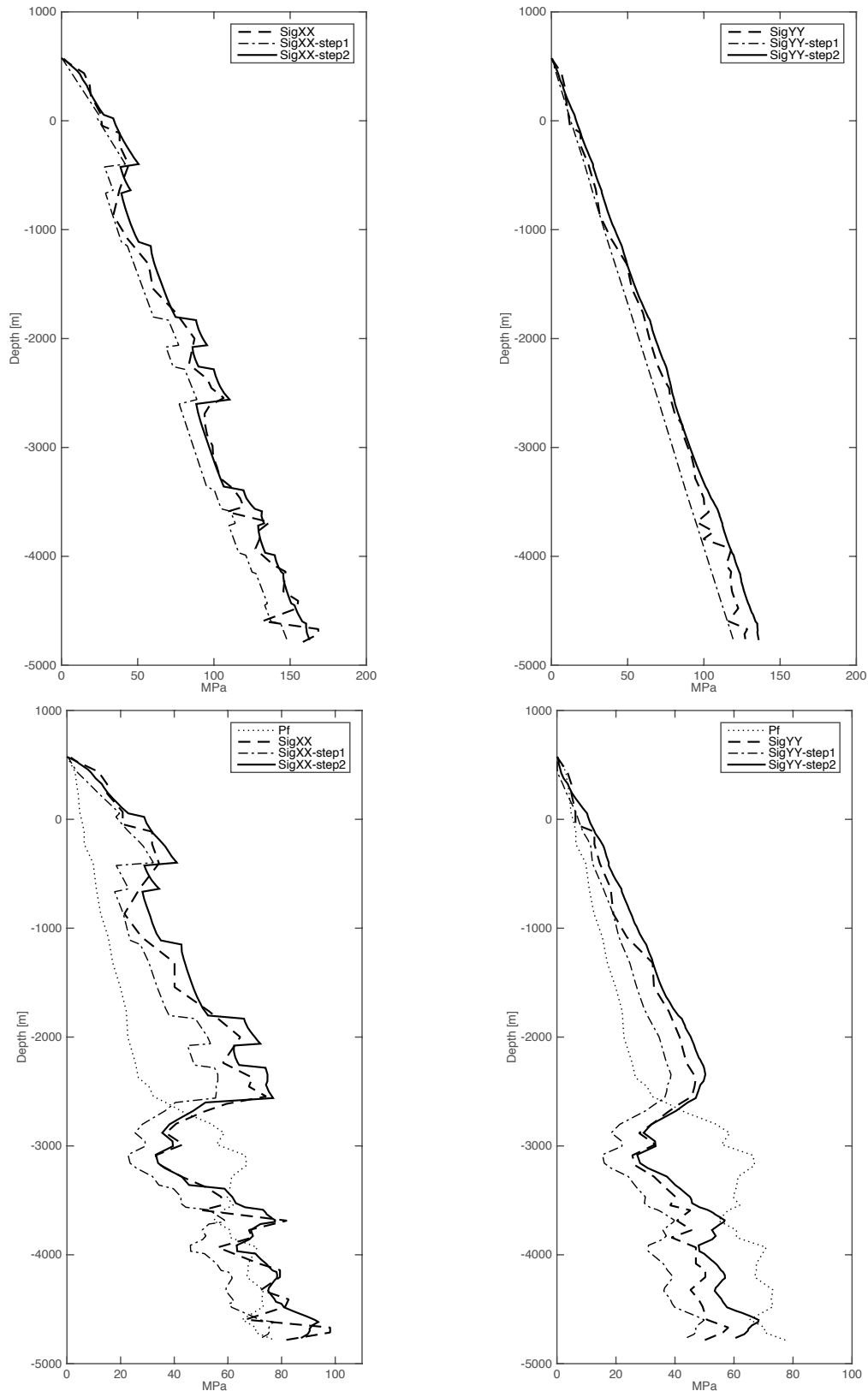


Figure 4 – Comparison of initial stress obtained using two-step procedure with available data: (Top-Left) total horizontal; (Top-Right) total vertical stress; (Bottom-Left); effective horizontal stress; and (Bottom-Right) effective vertical stress. In bottom diagrams dotted line is the available fluid pressure P_f along the wellbore. In all diagrams: continuous line is final initial stress calculated after two-step procedure, dashed line is available data, and dotted-dashed line is intermediate stress obtained in step1 of the procedure.

5 CONCLUDING REMARKS

In the present paper, further developments of the stress initialization technique in geological media described previously in [4-5] have been described. This procedure, based on Airy stress functions, constitutes a step forward with respect the simplest procedure of the fictitious Poisson's ratio, widely used in engineering practice. The mentioned improvements include: (1) an isoparametric representation of the subdomains that allow more general geometries, (2) more realistic stress conditions over the subdomain and its boundaries, and (3) the use of non-linear laws in the re-equilibration step, in order to redistribute unrealistically high deviatoric stress that may appear in the stress proposal at specific areas near the surface.

The described procedure has been applied to the stress initialization of a real reservoir cross-section where wellbore measurements were available. The same example was also used in the previous papers, and the results obtained with the new improvements show a better fit of both the stress proposal and the equilibrated stress states.

ACKNOWLEDGEMENTS

The work was partially supported by research grants BIA2016-76543-R from MEC (Madrid), which includes FEDER funds, and 2014SGR-1523 from Generalitat de Catalunya (Barcelona). Support from REPSOL for this research is also gratefully acknowledged. The first author acknowledges his FI doctoral fellowship received from AGAUR-Generalitat de Catalunya (Barcelona).

REFERENCES

- [1] Brown, E.T. and Hoek, E. Trends in relationships between measured in-situ stresses and depth. *International Journal of Rock Mechanics and Mining Sciences & Geomechanics Abstracts* (1978) **15**:211-215.
- [2] Fjaer, E., Holt, R. M., Raaen, A. M., Risnes, R. and Horsrud, P. Petroleum related rock mechanics. *Elsevier* (2008) **53**.
- [3] Parrish, D.K. and Labreche, D.A. Initializing The Equilibrium Stress state For Stress Analyses In Geomechanics. *The 29th US Symposium on Rock Mechanics (USRMS)* (1988).
- [4] Aliguer, I., Carol, I., Prat, P., Ybern, C.R., Lakshmikantha, M.R. and Segura, J.M. Numerical stress initialization in geomechanics via the FEM and a two-step procedure. *COMPLAS XIII: proceedings of the XIII International Conference on Computational Plasticity: fundamentals and applications, CIMNE* (2015) 667-676.
- [5] Aliguer, I., Ybern, C.R., Jaqués, I., Carol, I., Prat, P., Lakshmikantha, M.R. and Segura, J.M. Methods for FEM Stress Initialization Based on Stress Functions, and Application to a

Reservoir Cross-Section. *The 50th US Rock Mechanics/Geomechanics Symposium*, American Rock Mechanics Association (2016).

[6] Airy, G.B. On the Strains in the Interior of Beams. *Philosophical Transactions of the Royal Society of London* (1863) **153**:49-79.

[7] Timoshenko, S.P., Goodier, J.N. and Abramson, H.N. Theory of elasticity. *Journal of Applied Mechanics*. (1970) **37**:888.

[8] Drucker, D.C. and Prager, W. Soil mechanics and plastic analysis or limit design. *Quarterly of applied mathematics*. (1952) **10(2)**:157-165.